Errors in determination of soil water content using time-domain reflectometry caused by soil compaction around wave guides

Teamrat A. Ghezzehei

Earth Sciences Division, Lawrence Berkeley National Laboratory, Berkeley,

California, USA.

Teamrat A. Ghezzehei, Earth Sciences Division, Lawrence Berkeley National Laboratory, Berkeley, California, USA (TAGhezzehei@lbl.gov)

Abstract. Application of time-domain reflectometry (TDR) in soil hydrology often involves the conversion of TDR-measured dielectric permittivity to water content using universal calibration equations (empirical or physically based). Deviations of soil-specific calibrations from the universal calibrations have been noted and are usually attributed to peculiar composition of soil constituents, such as high content of clay and/or organic matter. Although it is recognized that soil disturbance by TDR wave guides may have impact on measurement errors, to our knowledge, there has not been any quantification of this effect. In this paper, we introduce a method that estimates this error by combining two models: one that describes soil compaction around cylindrical objects and another that translates change in bulk density to evolution of soil water retention characteristics. Our analysis indicates that the compaction pattern depends on the mechanical properties of the soil at the time of installation. The relative error in water content measurement depends on the compaction pattern as well as the water content and water retention properties of the soil. Illustrative calculations based on measured soil mechanical and hydrologic properties from the literature indicate that the measurement errors of using a standard three-prong TDR wave guide could be up to 10 percent. We also show that the error scales linearly with the ratio of rod radius to the inter-radius spacing.

1. Introduction

One of the attractive features of using time-domain reflectometry (TDR) for measurement of soil water content is the availability of universal calibration equations—which eliminates the need for soil-specific calibrations for most routine applications. Many of these calibration curves were derived by fitting empirical equations to large data sets of measured water content and dielectric permittivity [e.g., *Topp et al.*, 1980; *Schaap et al.*, 1996]. In addition, a few calibration equations are based on dielectric-mixing models [e.g., *Roth et al.*, 1990]. However, it has been noted that soil-specific calibration equations can significantly deviate from the universal calibrations for various reasons including effect of bound water and high organic matter content [see review by *Robinson et al.*, 2003].

In principle, water content measurement by TDR relies on spatially weighted volumetric averaging of dielectric permittivity of the medium surrounding the wave guides. Theoretical analysis of the transverse electromagnetic (TEM) wave propagation around the wave guides reveals that the regions closest to the wave guides have significantly higher weight than farther regions [*Knight*, 1992]. If the spatial distribution of dielectric around TDR wave guides is not uniform, then, the TDR-measured average dielectric permittivity differs from the arithmetic average. Sensitivity of a TDR system to complex distributions of water content around a probe as well as the effect of dielectric coatings were rigorously analyzed by *Ferre et al.* [1996, 1998]. Recently, *Hinnell et al.* [2006] analyzed the effect of heterogenous water content distribution caused by flow diversion around TDR rods.

Calculations of *Ferre et al.* [1998] indicate that the area sampled by various TDR probe designs is often restricted to a relatively small region surrounding the probes. Coinci-

dentally, this region is also the most impacted by soil disturbance during installation of the probes. The resulting alteration of water retention properties of the impacted soil induces systematic heterogeneity in the water content distribution very close to the wave guides. Therefore, the TDR-measured dielectric permittivity must be very sensitive to such compaction effects. The objective of this paper is to introduce a combined mechanical-hydrological approach for assessing measurement errors that are inherent in TDR-based water content determination.

2. Theoretical Considerations

In this section, we present a method for estimating TDR measurement errors that arise because of soil compaction during installation of the wave guides. In this method, modification of the soil structure is modeled using a soil compressibility theory introduced by *Farrell and Greacen* [1966]. The resulting change in porosity distribution is translated to evolution of water retention properties using an empirical method recently proposed by *Assouline* [2006]. Then, assuming the soil surrounding the TDR wave guides is under uniform matric potential we calculate the water content distribution. By combining the spatial water content distribution with the TEM wave propagation model [*Knight*, 1992], we then calculate the spatially weighted average permittivity sensed by the TDR. Finally, the compaction-related measurement error is evaluated as the deviation of the TDR-measured permittivity from average permittivity of the uncompacted soil.

2.1. Soil Compression by TDR Wave Guides

A large variety of TDR wave-guide designs have been used for various applications [e.g., *Robinson et al.*, 2003]. For brevity, this paper focuses only on the widely used three-prong

design illustrated in Figure 1a. The individual rods have circular cross-sections of radius a and are separated by a distance of S. The tip of each rod is assumed to be hemispherical in shape with radius of a. Soil compaction by the TDR rods will be evaluated by considering spherical stress distributions around the hemispherical tips [*Farrell and Greacen*, 1966]. The underlying assumption of this approach is that the void occupied by a TDR rod is created by the hemispherical tip as it is pushed through during installation. The derivation given in the remainder of this subsection (2.1) is based on the work of *Farrell and Greacen* [1966] and *Greacen et al.* [1968].

At equilibrium, the stress distribution around the hemispherical tip must satisfy

$$\frac{\partial \sigma_r}{\partial r} = -2\frac{\sigma_r - \sigma_t}{r} \tag{1}$$

where σ_r and σ_t are the radial and tangential stresses, respectively, and r is the spherical coordinate. Depending on the magnitude of the stress, the soil surrounding the TDR rods can be divided into two regimes of compaction. The inner most zone, which is subjected to stress greater than a certain threshold, undergoes plastic deformation whereas the far-field zone deforms elastically.

Assuming the soil is cohesive frictional material, σ_r and σ_t in the plastic zone ($r \leq R$) are related by

$$\sigma_t = \frac{1 - \sin\beta}{1 + \sin\beta}\sigma_r - \frac{2\cos\beta}{1 + \sin\beta}c \tag{2}$$

where c is cohesion and β is angle of internal friction. The solution to Eq. (1) that satisfies the stress relation of the plastic zone (2) is

$$\sigma_r = A(1 + \sin\beta)(R/r)^{4\sin\beta/(1+\sin\beta)} - c\cot\beta \tag{3a}$$

$$\sigma_t = A(1 - \sin\beta)(R/r)^{4\sin\beta/(1+\sin\beta)} - c\cot\beta \tag{3b}$$

where $r = R$ denotes the outer bound of the plastic zone and A is a constant that has to be determined.

In the elastic zone ($r > R$), the stresses induced by an internal pressure P_i generated at $r = R$ are distributed according to

$$\sigma_r = -P_i R^3 / r^3 \tag{4a}$$

$$\sigma_t = P_i R^3 / (2r^3) \tag{4b}$$

Assuming continuity of stresses at the plastic-elastic interface ($r = R$), we can use equations (3) and (4) to derive expressions for A and P_i

$$A = \frac{3c \ \cot\beta}{3 - \sin\beta} \tag{5a}$$

$$P_i = -\frac{4 \ c \cos\beta}{3 - \sin\beta} \tag{5b}$$

Further utilization of the above stress equations to determine soil compaction requires knowledge of the soil compressibility characteristics, which can be derived from experimental compression–load relations. The compression tests that are appropriate for describing soil deformation around rods driven into soil must be performed under failure [*Farrell and Greacen*, 1966]. A typical compression–load relationship under failure is illustrated in Figure 2. Based on such relationship, the zone of plastic deformation can be further subdivided into three subzones (also see Figure 1b) that are characterized by linear relationships between the voids-ratio (e) and the major principal stress (σ_r) in a log-linear plot. Within the central core of radius $r \leq R_m$, the soil is compressed to its minimum void ratio e_m while the stress exceeds σ_m. In the intermediate subzone (R_m–R_b), the soil is compressed under failure and the relation describing the compaction is referred to as the voids ratio at failure (VRF) line by *Farrell and Greacen* [1966]. In the outer

zone (R_b to R), the major and minor principal stresses are assumed to be related by the plastic failure condition and the relation describing such compaction is commonly known as rebound line. In summary the compression-load relations in the plastic zone can be mathematically described using,

$$e = \begin{cases} e_m & \sigma > \sigma_m \\ e_b + J\ \log(\sigma/\sigma_b) & \sigma_m \geq \sigma \geq \sigma_b \\ e_b + I\ \log(\sigma/\sigma_b) & \sigma_b > \sigma \geq P_i \end{cases} \tag{6}$$

where I and J are the compressibility indices for the rebound line and the VRF line, respectively.

In the elastic zone, the change in porosity ($\Delta\varphi$) is described by,

$$\Delta\varphi = P_i \frac{R^3}{r^3} \frac{1-\nu}{E} \tag{7}$$

where ν is Poisson's ratio and E is Young's modulus.

To complete the description of soil compaction around the TDR rods, we need to locate the boundary between the plastic and elastic zones (find the value of R). To accomplish this, we compare the distribution of pore space before and after the TDR probe is inserted as

$$\pi R^2 \varphi_\circ = \pi a^2 + \int_a^R 2\pi r\varphi\ dr - \int_R^\infty 2\pi r \Delta\varphi\ dr \tag{8}$$

where $\varphi = e/(1+e)$ is the porosity and $\varphi_\circ$ is the initial porosity. Note that this integration is performed for a cylindrical portion of the rod behind the tip. The left-hand-side denotes the total void space of the plastic zone before it is compacted. The first two terms in the right-hand-side represent the space occupied by the rod and the remaining pore space in the plastic zone, respectively. The last term denotes the change in total pore volume in the elastic zone. The value of R can now be calculated by evaluating the integrals in Eq.

(8). Note that the length quantities in Eq. (8) can be scaled by a allowing determination of R/a as a parameter that depends only on the soil properties.

Finally, the bulk density (ρ) distribution around TDR rods can be calculated using equations (6) and (7) as

$$\rho = \rho_p \begin{cases} 1 - e/(1+e)\,, & r \le R \\ 1 - (\varphi_\circ - \Delta\varphi)\,, & r > R \end{cases} \tag{9}$$

where ρ_p is the particle density.

2.2. Alteration of Soil Water Retention Curve

A significant consequence of change in soil bulk density is the alteration of the water retention characteristic (WRC)—the relationship between matric potential ψ and volumetric water content θ. Recently, *Assouline* [2006] introduced empirical relations that predict evolution of WRC as a function of change in bulk density for the WRC models of *Assouline et al.* [1998] and *Brooks and Corey* [1964]. The WRC model of *Assouline et al.* [1998] is given by

$$\Theta = 1 - \exp\left[-\alpha(\psi^{-1} - \psi_\circ^{-1})\right]^\mu \tag{10}$$

where $\psi_\circ = 1500\,\mathrm{kPa}$ is usually taken as the lowest matric potential limit and $\Theta = (\theta - \theta_r)/(\theta_s - \theta_r)$ is the effective saturation (with θ_s as the satiated θ and θ_r as the residual θ). This equation contains four free parameters that have to be estimated for each soil, θ_s, θ_r, μ, and α. The following set of empirical models predict evolution of these free parameters as a function of bulk density [*Assouline*, 2006]:

$$\theta_s/\theta_{s\circ} = (\rho_\mathrm{p} - \rho)/(\rho_\mathrm{p} - \rho_\circ) \tag{11a}$$

$$\theta_r/\theta_{r\circ} = \rho/\rho_\circ \tag{11b}$$

$$\alpha/\alpha_\circ = (\rho/\rho_\circ)^{3.72} \tag{11c}$$

$$\mu/\mu_\circ = (\rho/\rho_\circ)^\omega \tag{11d}$$

where the parameters with the subscript $\circ$ represent the initial (uncompacted) state. The parameter ω depends on the fractions of silt (F_{Sl}) and clay (F_{Sl}) by

$$\omega = 2.3 - 1.9/\sqrt{F_{\mathrm{Sl}}/F_{\mathrm{Cl}}} \tag{12}$$

If we assume the matric potential of the soil surrounding the TDR rods is uniform (steady state flow), we can calculate the water content distribution around the rods by substituting equations (9) and (11) in Eq. (10). The effect of matric potential heterogeneity because of flow diversion around the rods is negligible [*Hinnell et al.*, 2006].

2.3. Simulation of TDR Measurement

Water content measurement by the TDR method relies on spatially weighted averaging of the effective dielectric permittivity ε_r of the soil surrounding the TDR rods. The weight given to any location around the rods depends on the electric field intensity around the probes. In general, the electrostatic potential (ϕ) on any plane normal to the TDR rods satisfies the heterogeneous Laplace equation [e.g., *Knight*, 1992; *Robinson et al.*, 2003]

$$\nabla(\varepsilon_r(x,y)\nabla\phi) = 0 \tag{13}$$

where $\varepsilon_r(x,y)$ is local effective dielectric permittivity, which depends on the volume fractions of solids, gas, and water. We assume theoretical dielectric mixing is applicable for describing $\varepsilon_r(x,y)$. Particularly, we use the model of *Roth et al.* [1990] (see also *Jones et al.* [2002]),

$$\varepsilon_r = \{8\,\theta(x,y) + [2 - \varphi(x,y)]\}^2 \tag{14}$$

Knight [1992] defined the spatial weighting function that TDR wave guide rods sense as

$$w(x,y) = \frac{E^2}{\iint_A E^2\, dA} \tag{15}$$

where $E = |\nabla\phi|$ is the electric field intensity. Although Eq. (15) can be solved analytically only for limited conditions [*Knight*, 1992], it can be readily solved numerically using Finite-Element method. However, because of the steep slope of ϕ in the vicinity of TDR rods, numerically evaluated weighting function is very sensitive to the details of the model grid. Such errors were minimized in this study by increasing mesh density until stable distribution of w was obtained.

The average dielectric permittivity sensed by the TDR rods, for a particular transverse plane, can be calculated as

$$\varepsilon_{\mathrm{TDR}} = \iint_A w(x,y)\, \varepsilon_r(x,y)\, dA \tag{16}$$

Assuming the density and water content heterogeneities along the axes of the TDR rods are negligible, Eq. (16) also represents the average permittivity of the volume of soil surrounding the TDR rods.

Notice that, if the effects of the TDR rods on the soil density and water content surrounding the rods can be ignored (e.g., by installing TDR probes in to pre-drilled holes), then the permittivity is uniform everywhere, $\varepsilon_r(x,y) = \varepsilon_{r\circ}$. Hence, Eq.(16) is reduced to

$$\varepsilon_{\mathrm{TDR}} = \varepsilon_{r\circ} \tag{17}$$

Soil-specific calibrations of TDR water content measurement systems can be developed using relationships between $\varepsilon_{\mathrm{TDR}}$ and bulk water content ($\theta_\circ$). Alternatively, the spatially averaged permittivity $\varepsilon_{\mathrm{TDR}}$ can be translated to water content using one of several gener-

alized conversion equations (empirical and theoretical). For consistency, we will use the inverse of Eq. (14) to calculate θ_{TDR},

$$\theta_{\mathrm{TDR}} = \frac{\sqrt{\varepsilon_{\mathrm{TDR}}} - (2 - \varphi_{\circ})}{8} \tag{18}$$

Notice that if soil compaction by TDR rods was negligible, Eq. (17) leads to

$$\theta_{\mathrm{TDR}} = \theta_{\circ} \tag{19}$$

In the remainder of this paper, we refer to this simulated water content measurements (θ_{TDR}) as "TDR-measured water content". Now, we can define the relative error induced by soil compaction as

$$\epsilon = \frac{\theta_{\mathrm{TDR}} - \theta_{\circ}}{\theta_{\circ}} 100 \tag{20}$$

This error can be attributed only to compaction because the same mixing model is used to relate water content and permittivity locally (Eq. (14)) and macroscopically (Eq. (18)). As it will be shown in the subsequent illustrative examples, the magnitude of the error depends on water content and soil mechanical properties.

3. Illustrative Examples

3.1. Soil Properties

To illustrate the method of estimating compaction-related TDR measurement error, we use mechanical and hydrological properties of the Parafield soil reported by *Farrell and Greacen* [1966] and *Greacen et al.* [1968]. Surface soil that passed through 2 mm was compacted into brass cylinders until the desired bulk density (1500 kg/m^3, 1600 kg/m^3, or 1700 kg/m^3) was achieved. The samples were wet by capillary rise from a suction plate and subsequently drained to 30 kPa and 70 kPa matric potentials. The equilibrium water contents at the respective suctions are given in Table 1. These measured data along

with fitted *Assouline et al.* [1998] WRC model are shown in Figure 3. The model WRC at $\rho_b = 1500\,\mathrm{kg/m^3}$ was obtained by fitting Eq. (10) to the measured data. For the remaining densities, the WRC parameters were calculated using Eq. (11). The good match between the modeled and measured WRC at $\rho_b = 1600\,\mathrm{kg/m^3}$ and $\rho_b = 1700\,\mathrm{kg/m^3}$ as an indication the WRC evolution model of *Assouline* [2006] is applicable for the Parafield soil.

Subsequent to water content water measurement, the equilibrated cores were transferred to triaxial apparatus and subjected to tests that provided with cohesion (c), angle of internal friction (ϕ), Young's modulus (E), and the rebound and VRF lines. The resulting compression-load data along with fitted rebound and VRF lines are shown in Figure 4. The derived mechanical parameters are summarized in Table 1.

3.2. Effect of Probe Design on Measurement Errors

As indicated in sub-section 2.1, the relative location of the plastic-elastic zone boundary ($R^* = R/a$) depends only the mechanical properties of the soil but not on the radius of the rods. Consequently, the density distribution around the TDR rods also depends only on the dimensionless distance from the rod ($r^* = r/a$) but not the actual rod diameter. Similarly, the spatial weighing function (Eq. 15) depends only the relative distance from the TDR rods (r^*). Therefore, the geometric effect of a three-rod TDR probe can be effectively described using the dimensionless spacing between the rods [c.f. *Knight*, 1992]

$$G = S/a \tag{21}$$

Similar relation also holds for two-rod TDR probe.

In the subsequent illustrative examples, we will focus only on a TDR probe made of three equal sized and equidistant rods. As the base-case TDR probe design, we use the

specifications of a commercial three-rod probe (Campbell Scientific Inc, Logan, UT) with rod diameter of $2\,a = 4.8\,\text{mm}$ and inter-rod spacing of $S = 22\,\text{mm}$. The corresponding geometric factor for the base case probe is $G = 9.167$.

In Figure 5, we illustrate the main steps involved in estimating compaction-related TDR measurement errors for two TDR designs—the base design with $G = 9.167$ (top row) and $G = 4.583$ (bottom row). The three columns in Figure 5 (ρ_b, θ, and normalized weight) are calculated sequentially from left to right. To allow direct comparison between probes of different G values, the distribution of the weighting function w was normalized with respect to the global maximum weight for the respective probe design.

If the overlap of the stress-fields of adjacent rods can be ignored, these distributions are truly dimensionless. For completeness, however, in Figure 5 and all subsequent examples the stresses due to all the individual rods were summed before the bulk density calculations were performed. The implications of overlapping stress-fields on the measurement-error will be elaborated further in the subsequent subsection. Note that a probe design with a value of $G = 4.583$ (which is half of the base design $G = 9.167$) could be achieved by either doubling the rod diameters or halving the inter-rod spacing. Irrespective of whether the stress-fields are overlapping, when the value of G is small, a large portion of the soil volume that surrounds a TDR probe is occupied by the rods—hence, the compaction effect is also more pronounced.

For the bulk density calculations (first column), we used the mechanical properties of the Parafield soil at initial bulk density and matric potential of $\rho_b = 1500\,\text{kg/m}^3$ and $\psi = 30\,\text{kPa}$, respectively. The water content and permittivity distributions were

calculated assuming the soil has equilibrated at matric potential of $\psi = 7.65\,\mathrm{kPa}$ (the soil is wetter than when the probes were installed).

Independent of the compaction effects, the propagation of the TEM is also significantly impacted by G [*Knight*, 1992]. In general, larger values of G indicate distribution of the electric-field intensity over a larger cross-sectional area. Conversely, when the value of G is smaller, only a smaller volume of soil that is in close contact with the TDR rods (which is compacted the most) impacts the TEM travel time and the resulting permittivity measurement. As a consequence of the combined effects of compaction and TEM propagation, TDR probes with small G are prone to more errors that arise because of compaction effects. However, the dependence of the weighting function on G would not have an impact if the water content is uniformly distributed (effect of compaction is negligible) within the volume of influence.

As indicated by the dashed horizontal line in Figure 3, compaction increases the proportion of pores that remain filled with water at the given matric potential value of $\psi = 7.65\,\mathrm{kPa}$. As a result, the water content is higher in the soil regions that are the closest to the rods as shown in the second column of Figure 5. Consequently, the permittivity measured by a TDR is larger than that of the far-field regions not mechanically affected by installation of the TDR probe.

Finally, it is very important to note that in the last column of Figure 5 the weighting decreases rather drastically with distance away from the TDR rods—the spacing between the contours of w is one order of magnitude. This strong bias towards the soil in contact with the TDR rods, which is also the most susceptible to compaction and water content alteration, is the major cause for the marked errors that we report in this paper.

3.3. Effect of Soil Properties on Measurement Errors

The water-content vs. permittivity relationships of certain soils (e.g., forest soils [*Schaap et al.*, 1996]) significantly deviate from the widely used universal calibrations . Such deviations are mostly attributed to the effect of soil constituents (such as organic matter and clay) on the dielectric permittivity (e.g., binding of water on clay surfaces). Here, we will show that the water content of the soil at the time of the TDR probe installation can also have an impact on the θ-$\varepsilon_{\mathrm{TDR}}$ relation through soil compaction around TDR rods. Moreover, these results also suggest that differences in soil mechanical and/or hydrological properties can lead to differences in their respective θ-$\varepsilon_{\mathrm{TDR}}$ relations.

In Figure 6, we show the distribution of bulk density around a single rod using the six combinations of initial ρ_b and ψ of Parafield soil given in Table 1), for which measured mechanical properties are available [*Farrell and Greacen*, 1966]. Recall that the stress distributions for all the six cases are identical. The differences in density arise because of the differences in the compression-load relationships of the soils at the various initial states. Because the differences in mechanical properties between the soils equilibrated at matric potentials of 30 kPa and 70 kPa are small, the corresponding differences in ρ_b are also small. However, the differences between the soils at different initial density are remarkable. In all the distributions, there is a marked change in the slope at the interface between the region compressed plastically along the VRF line (close to the probe) and the region compresses plastically along the rebound line. The interface between the plastic and elastic zones are not noticeable. Only the soil initially at $\rho_b = 1700\,\mathrm{kg/m^3}$ and 30 kPa was compressed until it reached the minimum voids-ratio limit. The absolute change in density is the largest for the $\rho_b = 1500\,\mathrm{kg/m^3}$ soils at the soil-rod interface. Moreover,

for these soils most of the rod-volume was accommodated by compaction along the VRF line within a short relative distance (r/a) from the rod. In contrast, for the densest soil a substantial proportion of the rod volume was distributed over a larger cross-sectional area. Note that the compression required to offset a given volume decreases with radial distance.

The simple density profiles we presented above do not consider the overlapping stress-fields of adjacent rods. The significance of the overlap can be readily noticed in Figure 6. The location of the midpoints between adjacent probes for the two wave-guide designs presented in Figure 5 ($G = 9.167$ and $G = 4.583$) are located at $r/a = 4.58$ and $r/a = 2.29$, respectively, and are marked by a vertical dashed lines in Figure 6. Note that the influence of the rod extends beyond the midpoint, especially for the probe with $G = 4.583$. The overlap also increases with the initial bulk density, because the compaction of harder soils is more spread out. Recall that the bulk density profiles shown in Figure 5 properly account for such overlaps because they were calculated using the sum of the stresses imposed by all the probes. However, the additional compaction because of the stress-field overlaps does not significantly contribute to the measurement errors.

In Figure 7 we present the predicted relative errors in the TDR-measured water content (calculated using 20) that arise because of compaction and the associated heterogeneity in water content around a TDR probe. Generally, compaction increases the proportion of the fine pores resulting in higher water content near the TDR rods when on average the soil is relatively dry. Thus, on the dry end of the water content range, the TDR-measured water content is higher than the average water content. Conversely, because compaction

reduces the proportion of relatively big pores, the TDR-measured water content is lower than the average.

Particularly, for Parafield soil and the base-case TDR probe, the estimated error can be as high as 10 %. Softer soils (with high water content and/or low density during probe installation) tend to have more compaction closer to the rods, which makes them more prone to errors.

Comparison of parts (a) and (b) of Figure 7 reveals that halving the geometric factor G approximately doubles the errors. The trend is to be expected as already described in subsection 3.2. Moreover, as an approximate rule of thumb, we can expect the error to linearly increase with $1/G$.

4. Conclusions

In this paper, we introduced a novel approach for quantifying the errors in water content measurement using TDR that can arise from compaction of the soil surrounding the wave guides during installation. Although the errors we calculated for illustrative purposes may not be quantitatively applicable to other soils, the following general conclusions and trends are expected to apply to most soils:

1. Installing TDR probes when the soil is soft, such as after irrigation or tillage, increases susceptibility to systematic errors.

2. By extension from the above, inherently soft soils are more likely to have higher errors.

3. In general, the effect of compaction is underestimation of water content when the soil is very wet and over estimation in mid- to low-range wetness.

4. The magnitude of the error is expected to increase with $1/G$.

The method presented in this paper can be readily adapted to other soil sensors that rely on volumetric averaging of quantities in the vicinity of a sensor, such as heat-dissipation probe. However, this method may not be applicable if the compaction and/or evolution of WRC models are inappropriate. For example, the compaction model may not accurately describe the density distribution in non-cohesive soils or soils with macropores in the order of the TDR rods. Moreover, inherent heterogeneity in density and/or WRC at the scale of the TDR rods could mask the effects of compaction. T

Acknowledgments. This work was supported by the U.S. Dept. of Energy under Contract No. DE-AC02-05CH11231. Critical reviews of an earlier version of the manuscript and suggestions for improvement by Dani Or, Rohit Salve, Stefan Finsterle and three anonymous reviewers are gratefully acknowledged.

References

Assouline, S., Modeling the relationship between soil bulk density and the water retention curve, *Vadose Zone Journal*, *5*(2), 554–563, 2006.

Assouline, S., D. Tessier, and A. Bruand, A conceptual model of the soil water retention curve, *Water Resources Research*, *34*(2), 223–231, 1998.

Brooks, R. H., and A. T. Corey, Hydraulic properties of porous media, hydrology paper no. 3, *Tech. rep.*, Civil Engineering Dept, University of Colorado, 1964.

Farrell, D., and E. Greacen, Resistance to penetration of fine probes in compressible soil, *Australian Journal of Soil Research*, *4*(1), 1–17 (doi:10.1071/SR9660,001), 1966.

Ferre, P. A., D. L. Rudolph, and R. G. Kachanoski, Spatial averaging of water content by time domain reflectometry: Implications for twin rod probes with and without dielectric coatings, *Water Resources Research*, *32*(2), 271–279, 1996.

Ferre, P. A., J. H. Knight, D. L. Rudolph, and R. G. Kachanoski, The sample areas of conventional and alternative time domain reflectometry probes, *Water Resources Research*, *34*(11), 2971–2979, 1998.

Greacen, E., D. Farrell, and B. Cockrift, Soil resistance to metal probes and plant roots, in *Australian Journal of Soil Research*, pp. 769–779, Trans. 9th Int. Cong. Soil Sci. I, Angus and Robertson, Sydney, 1968.

Hinnell, A. C., T. P. A. Ferre, and A. W. Warrick, The influence of time domain reflectometry rod induced flow disruption on measured water content during steady state unit gradient flow, *Water Resources Research*, *42*(8), W08,420, 2006.

Jones, S. B., J. M. Wraith, and D. Or, Time domain reflectometry measurement principles and applications, *Hydrological Processes*, *16*(1), 141–153, 2002.

Knight, J. H., Sensitivity of time domain reflectometry measurements to lateral variations in soil-water content, *Water Resources Research*, *28*(9), 2345–2352, 1992.

Robinson, D. A., S. B. Jones, J. M. Wraith, D. Or, and S. P. Friedman, A review of advances in dielectric and electrical conductivity measurement in soils using time domain reflectometry 10.2113/2.4.444, *Vadose Zone J*, *2*(4), 444–475, 2003.

Roth, K., R. Schulin, H. Fluhler, and W. Attinger, Calibration of time domain reflectometry for water-content measurement using a composite dielectric approach, *Water Resources Research*, *26*(10), 2267–2273, 1990.

Schaap, M. G., L. de Lange, and T. J. Heimovaara, TDR calibration of organic forest floor media, *Soil Technology*, *11*, 205217, 1996.

Topp, G. C., J. L. Davis, and A. P. Annan, Electromagnetic determination of soil water content: Measurements in coaxial transmission lines, *Water Resources Research*, *16*(3), 574582, 1980.

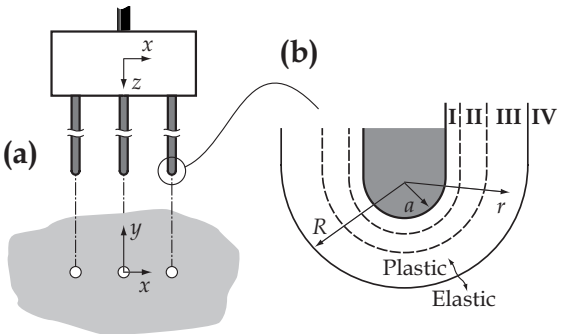

Figure 1. Geometric definitions (a) of the Cartesian coordinate system and (b) schematic arrangement of the plastic and elastic zones and subzones.

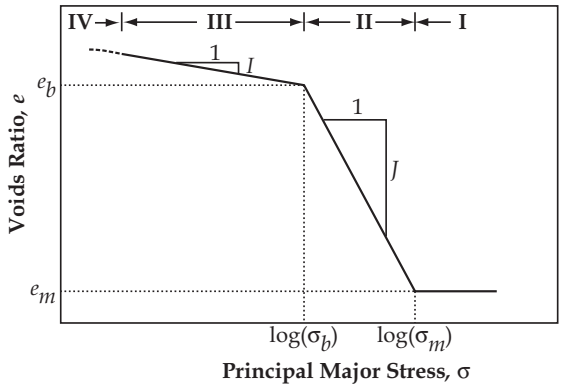

Figure 2. Schematic relationship between the principal major stress (σ_r) and voids-ratio e (adapted from *Farrell and Greacen* [1966]).

Table 1. Mechanical and hydrologic properties of Parafield soil based on measured data from *Farrell and Greacen* [1966] and fits of water retension characteristic model of *Assouline et al.* [1998].

		Bulk Density, ρ_b (kg/m^3)					
		1500		1600		1700	
Mechanical and Hydrologic Parameters Derived from *Farrell and Greacen* [1966]							
ψ	(kPa)	0.3	0.7	0.3	0.7	0.3	0.7
θ	(m^3/m^3)	0.18	0.16	0.19	0.17	0.20	0.18
c	(kPa)	7.85	11.8	11.8	16.7	15.7	22.6
E	(MPa)	18.6	–	21.6	–	23.5	24.5
β	(deg)	37	39	39	40	41	41
$e_\circ$	(m^3/m^3)	0.764	0.764	0.654	0.654	0.556	0.556
e_b	(m^3/m^3)	0.754	0.750	0.641	0.637	0.535	0.531
e_m	(m^3/m^3)	0.39	0.39	0.39	0.39	0.39	0.39
σ_b	(kPa)	56.10	100.9	140.28	252.35	331.13	595.66
σ_m	(kPa)	1083	1887	1083	1887	1083	1887
R/a	–	8.27	8.80	9.79	10.6	9.66	9.11
Parameters of the *Assouline et al.* [1998] WRC Model							
α	(kPa)	4.80[a]		6.10[b]		7.65[b]	
μ	–	0.8178[a]		0.8558[b]		0.8931[b]	
θ_r	(m^3/m^3)	0.149[a]		0.159[b]		0.168[b]	
θ_s	(m^3/m^3)	0.434[a]		0.396[b]		0.358[b]	

[a] Optimized by fitting Eq. (10) to measured ψ vs. θ data.

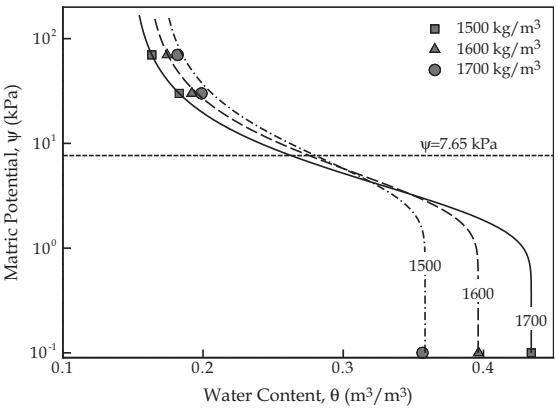

Figure 3. Water retention characteristics (WRC) of Parafield soil based on measured water content and matric potential data of *Farrell and Greacen* [1966]. The measured data at $1500\,\mathrm{kg/m^3}$ were fitted with the WRC model of *Assouline et al.* [1998] given by Eq. 10. The WRC model curves for $1600\,\mathrm{kg/m^3}$ and $1700\,\mathrm{kg/m^3}$ were predicted using Eq. 11. The parameters of the model are given in Table 1

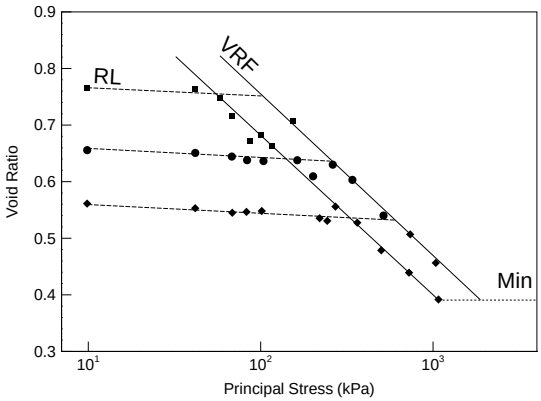

Figure 4. Relationship between the principal major stress (σ_r) and voids-ratio e for Parafield soil at three initial bulk densities (■ = $1500\,\mathrm{kg/m^3}$, • = $1600\,\mathrm{kg/m^3}$, and ♦ = $1500\,\mathrm{kg/m^3}$) and two matric potentials ($\psi = 30\,\mathrm{kPa}$ and $\psi = 70\,\mathrm{kPa}$) (based on measured data and model parameters reported by *Farrell and Greacen* [1966]).

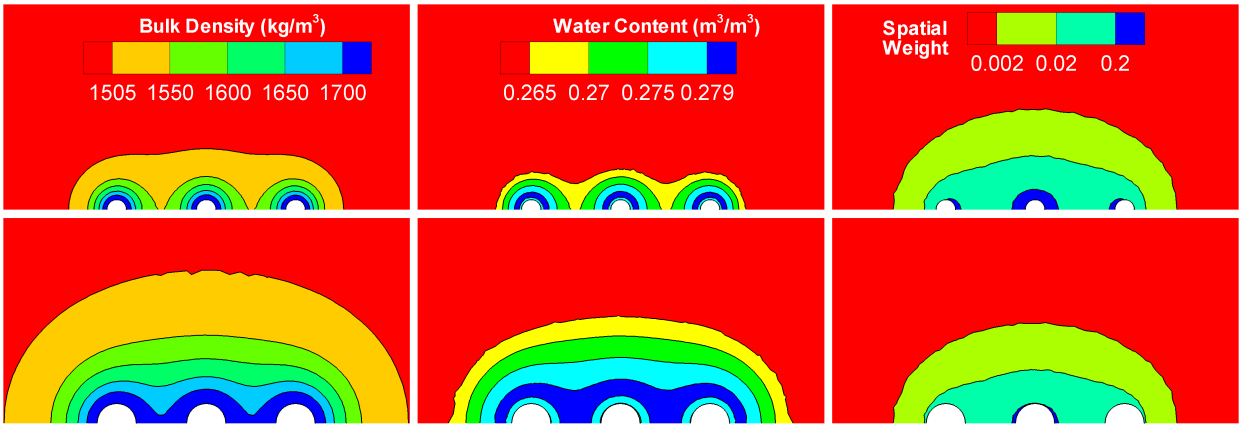

Figure 5. Spatial distributions of bulk density, water content, and TDR weighting function for a standard three-prong TDR wave guide (Upper row) and a similar probe but with twice as thick rods (lower row).

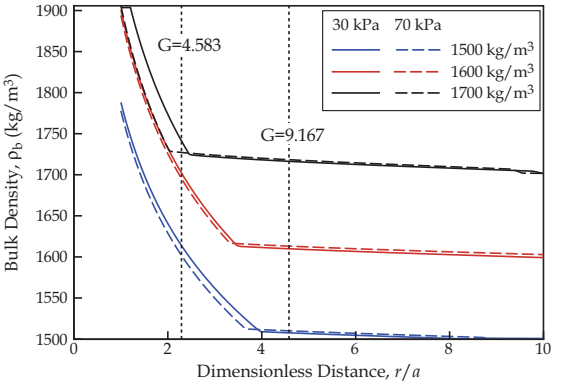

Figure 6. Soil bulk density distribution around a single rod as a function of dimensionless distance (r/a) for six combinations of initial soil bulk density and matric potential.

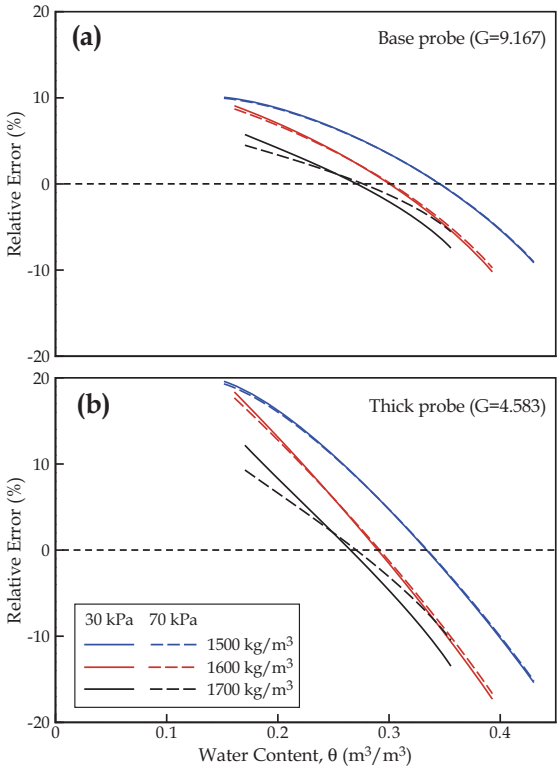

Figure 7. Relative errors in water content measurement for (a) the base-case TDR probe design with $G = 9.167$ and (b) the modified probe design with $G = 4.583$.